Preparation and Photocatalytic Performance of p-n Heterojunction Photocatalyst Bi_2O_3/TiO_2

Shengqing Wang · Biyang Tuo (ID) · Jianli Wang · Yun Tang · Guanghua Nie · Fei Xie

Abstract The p-n heterojunction Bi_2O_3/TiO_2 catalysts with different mass ratios of Bi_2O_3 were prepared by the sol–gel method. Under simulated solar irradiation, the photocatalytic degradation effects of Bi_2O_3, TiO_2, and p-n heterojunction Bi_2O_3/TiO_2 on acid red 18 (AR18) were evaluated. The characterizations show that the diffraction peaks were all anatase phase and Bi_2O_3 was evenly distributed on the surface of TiO_2. With the increase of Bi_2O_3 content, the band gap of the composites gradually decreased. When the dosage of catalyst (Bi_2O_3 mass ratio was 10%) was 0.5 g/L and the initial concentration of dye was 50 mg/L, the photocatalytic experiment was carried out under a xenon lamp (500 W), the p-n heterojunction formed by Bi_2O_3 and TiO_2 improved the performance of the photocatalyst and showed good catalytic performance under acidic conditions. Compared with TiO_2 and Bi_2O_3, when the mass ratio of Bi_2O_3 was 10%, the photocatalytic degradation performance of the material was the best, and the degradation rate of AR18 could reach 99.76% after 210 min illumination.

Keywords Bi_2O_3/TiO_2 · Sol–gel method · Photochemical catalysis · p-n heterojunction · AR18

S. Wang · B. Tuo (✉) · Y. Tang · G. Nie · F. Xie
College of Mining, Guizhou University, Guiyang 550025, People's Republic of China
e-mail: bytuo@gzu.edu.cn

B. Tuo · Y. Tang · G. Nie · F. Xie
National and Local Joint Laboratory for Effective Utilization of Mineral Resources in Karst Area, Guiyang 550025, People's Republic of China

J. Wang (✉)
College of Metallurgy and Material Engineering, Hunan University of Technology, Zhuzhou 412000, People's Republic of China

1 Introduction

In recent years, environmental problems for instance water pollution have drawn a lot of attention. Azo dyes (such as acid ed 18, reactive black 5, direct yellow 27, etc.) are those containing azo (–N=N–) groups that can lead to low biodegradability, and therefore, many risks are posed to ecosystems and human health (Luo et al., 2022a, 2022b, 2022c, 2022d). Therefore, how to remove organic dyes before they are discharged into the water environment is extremely significant for water treatment. Traditional water treatment methods cannot effectively degrade these persistent organic pollutants (POPs) in wastewater (Mejía-Morales et al., 2020; Mishra et al., 2022). Photocatalytic degradation technology has great potential as a promising environmental purification method to solve the problem of dye pollution in the water environment (Luo et al., 2022a, 2022b, 2022c, 2022d).

N-type semiconductor material TiO_2 dominated by electronic conductivity has become the most widely used photocatalyst, because of its low cost, stability,

low toxicity, and environmental friendliness (Ge et al., 2021; Khalid et al., 2017). Nevertheless, the practical application of TiO_2 in wastewater treatment mainly has the following problems: (1) photogenerated electron–hole pairs are easy to recombine, resulting in reducing photocatalytic performance (Răileanu et al., 2013); (2) TiO_2 particles are easy to agglomerate during the photodegradation process, which hinders the light absorption and reduces the photocatalytic performance (Cervantes-Aviles et al., 2017); and (3) the wide band gap (> 3.2 eV) of TiO_2 results in its low utilization of sunlight, hindering the application of TiO_2 in practical photodegradation (Arutanti et al., 2022). The construction of heterojunction is an effective method to solve the above problems (Low et al., 2017; Taddesse et al., 2020; Wu et al., 2022). P-type semiconductor Bi_2O_3 with hole-conductivity as the main component has good photosensitivity. In addition, during the calcination process, Bi^{3+} easily combines with O_2 to form Bi_2O_3 (Ren et al., 2015). Therefore, p-type semiconductor Bi_2O_3 and n-type semiconductor TiO_2 are selected to construct heterojunction, which is helpful for the effective separation of photogenerated carriers and the improvement of photocatalytic activity (Meda et al., 2022; You et al., 2021).

In this paper, composites with different mass ratios of Bi_2O_3 were prepared by the sol–gel method, and the effect of Bi_2O_3 content on the final catalytic performance of the materials was discussed. Bi_2O_3 is uniformly distributed on bulk TiO_2 to provide high-density active sites. The p-n heterojunction Bi_2O_3/TiO_2 ensures the separation of electrons of Bi_2O_3 and holes of TiO_2 and has a strong redox ability. To evaluate the photocatalytic degradation activity of p-n Bi_2O_3/TiO_2, the degradation effect of AR18 was observed under full-spectrum light.

2 Experiment

2.1 Material Preparation

The reagents bismuth nitrate pentahydrate (Bi $(NO_3)_3 \cdot 5 H_2O$), nitric acid (HNO_3), acetic acid (CH_3COOH), tetrabutyl titanate ($C_{16}H_{36}O_4Ti$), ethanol (C_2H_5OH), acid red 18 (AR18), ammonia water, and pure TiO_2 for anatase purchased in Macklin are analytically pure.

A 5-mmol Bi $(NO_3)_3 \cdot 5H_2O$ was dissolved in dilute nitric acid solution. At room temperature, 32 mL ammonia water was added to bismuth nitrate pentahydrate solution by drop (Cheng & Kang, 2014). The generated suspension was treated with ultrasound to reduce agglomeration, and Bi_2O_3 powder was obtained by filtration drying and calcination at 550 ℃.

A certain amount of bismuth nitrate pentahydrate was dissolved in nitric acid solution to obtain liquid B. Twenty milliliters of tetrabutyl titanate and 20-mL anhydrous ethanol were mixed, and 6-mL glacial acetic acid was added and stirred for 30 min to obtain liquid A (Xiang et al., 2021). The sol was formed by slowly dropping liquid B into liquid A, and the wet gel was obtained after aging at room temperature for 24 h. After drying at 80 ℃, the wet gel was ground to 0.075 mm, and the composite Bi_2O_3/TiO_2 was obtained after calcination at 450 ℃ for 1 h (Vigil-Castillo et al., 2019). TB05, TB10, TB20, and TB30 will contain 5 wt %, 10 wt %, 20 wt %, and 30 wt % Bi_2O_3.

2.2 Characterization of Materials

X-ray diffractometer (XRD, Rigaku Smart Lab SE, Japan) was used to test at the scanning rate of 2 ℃/min under Cu-Kα radiation, 40 kV, and 40 mA. Raman spectra of materials were recorded using a Raman microscope (Renishaw in Via, England) with a laser diode (780 nm) as source of radiation. The surface morphology of the catalyst was analyzed by scanning electron microscopy (SEM, ZEISS Sigma 300, Germany), and the elemental composition of the material was recorded by energy-dispersive X-ray spectrometer (EDS, Hitachi Ltd., Japan). The materials' diffuse reflectance spectra (UV–vis DRS) in the wavelength range of 200–800 nm was measured on the UV-3600i Plus spectrophotometer (Shimadzu, Japan) to analyze the light absorption characteristics of the material. The absorbance of acid red 18 wastewater was measured by UV spectrophotometer (UV–Vis, TU-1901, China). Electron paramagnetic resonance (EPR) was performed on ESR spectrometer (Bruker EMX PLUS, Germany) with a modulation frequency of 100 kHz. Zeta potential data was measured with a 90Plus PALS high sensitivity zeta potential and particle size analyze (DelsaNanoC, USA).

2.3 Adsorption Study

The composite (0.05 g) was placed in the AR18 solution (100 mL, 50 mg/L) and stirred in a dark box for 30 min. Five milliliters of the solution was sampled every 5 min. Post-centrifugation, the absorbance of the AR18 solution was measured at a wavelength of 508 nm. The amount of AR18 adsorbed by the composite could be calculated by using Eqs. 2–1:

$$Q_t = \frac{(C - C_t)V}{m} \qquad (2\text{-}1)$$

where t is adsorption time (min), Q_t is the amount of adsorption at time t (mg/g), C is the initial concentration of the AR18 solution (mg/L), C_t is the concentration of AR18 solution at time t (mg/L), V is the initial volume of the AR18 solution (L), and m is the weight of the composite (g).

2.4 Photocatalytic Performance Test

A 500-W xenon lamp was used to simulate the sunlight, and the target pollutant AR18 was irradiated and catalytically degraded. The photocatalytic properties of a series of Bi_2O_3/TiO_2 composites with different mass ratios were tested. The ambient temperature was maintained by circulating cooling water, and the light source was located 10 cm above the reaction vessel. The reaction device is shown in Fig. 1. In the photocatalytic experiment, a 50-mg catalyst was added into 100 mL AR18 solution (50 mg/L) and stirred for 30 min in dark environment to achieve adsorption equilibrium. After the beginning of the light reaction, about 5-mL suspension
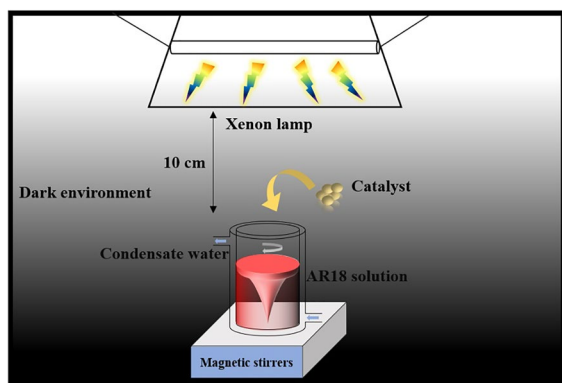

Fig. 1 Photocatalytic device schematic

was centrifuged every 30 min to remove the catalyst, and the supernatant was measured by ultraviolet spectrophotometer at 508 nm. The degradation rate of AR18 was calculated according to the following Eq. 2–2.

$$\eta = \frac{A - A_m}{A} = \frac{C_0 - C_m}{C_0} \times 100\% \qquad (2\text{-}2)$$

where m is photocatalytic reaction time (min), A is initial absorbance of solution (a. u), A_m is the absorbance of solution after photocatalytic reaction for time m, (a. u), C_0 is initial solution concentration (m/L), and C_m is the concentration of solution after photocatalytic reaction for time m (mg/L).

3 Result and Discussion

3.1 Morphology, Structure, and Optical Properties of Catalysts

The crystal structure of the photocatalyst was tested by XRD. From Fig. 2a, when the 2θ values are 25.06°, 37.80°, 48.00°, 53.88°, 62.88°, 68.7°, and 75.02°, strong diffraction peaks appear, which are all from 101, 004, 200, 105, 204, 116, and 215 crystal planes of TiO_2 anatase phase (JCPPDS21-1272). There were no diffraction peaks of Bi_2O_3 in TB10, TB20, and TB30. For TB10 and TB20, it was due to the low content of Bi_2O_3, which did not meet the detection limit of XRD. However, 30% content of Bi_2O_3 could not be detected by XRD, and this phenomenon could result from the amorphous structure of Bi_2O_3 (Valencia et al., 2018). It is common that the Bi_2O_3 crystal phase in Bi/Ti composites cannot be identified (Lou et al., 2021; Rongan et al., 2020; Tang et al., 2021; Zhang et al., 2021a, 2021b). Bi_2O_3 has four crystal phases: α, β, γ, and δ. According to the different synthesis methods, Bi_2O_3 was combined with TiO_2 with different crystal phases. On the other hand, due to the different ionic radius of Ti^{4+} (68 pm) and Bi^{3+} (96 pm), Bi^{3+} cannot replace Ti^{4+} in TiO_2 lattice, nor can it be incorporated into anatase lattice. Compared with TiO_2 standard card, the positions of diffraction peaks of TB10, TB20, and TB30 had no obvious shift, which is also confirmed. With the gradual increase of Bi_2O_3 content, the white of the material gradually changed from pure TiO_2 to light yellow of
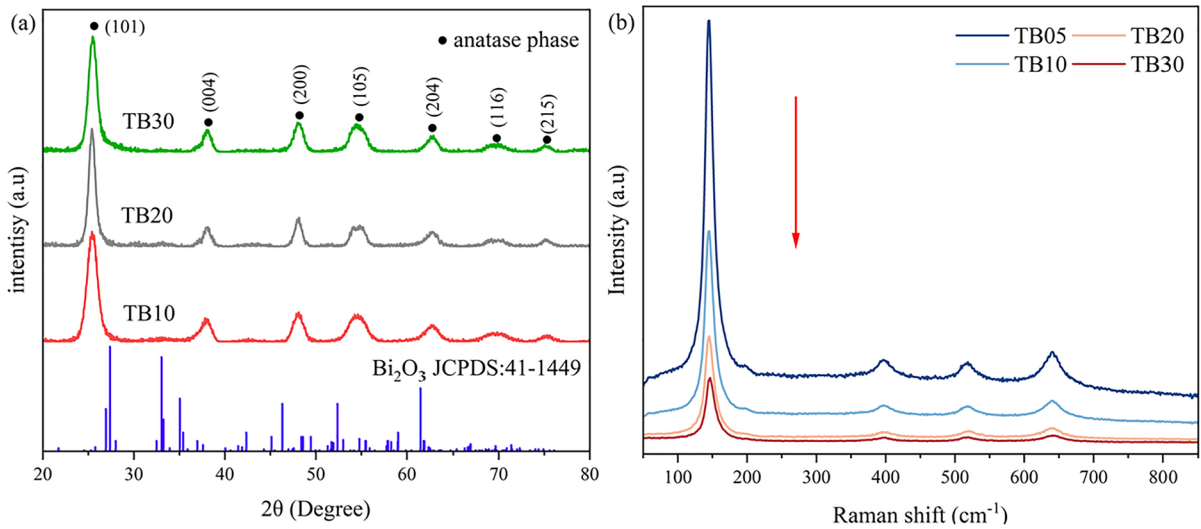
Fig. 2 XRD of TB10, TB20, and TB30 samples (**a**). Raman spectra for TB05, TB10, TB20, and TB30 (**b**)

TB05, TB10, TB20, and TB30, which also confirms the combination of TiO₂ and Bi₂O₃. The content of bismuth in TB05, TB10, TB20, and TB30 tested by the thiourea method was about 4.2%, 8.4%, 17.6%, and 26.5%, respectively, accounting for more than 80% of the theoretical value.

The Raman spectra obtained of synthesized materials are concordant with the results obtained by XRD. In Fig. 2b, the Raman spectra shows signals attributed only to anatase phase (143, 194, 394, 516, 637 cm⁻¹) were observed (Vigil-Castillo et al., 2019). It can be found that with the increase of Bi₂O₃ content in the material, the signal of anatase in the graph drifts to a smaller wavelet number, and the peak was weak. This confirms Bi₂O₃ dispersion in TiO₂, and it is concordant with the inhibition of growth of anatase crystallites (Yi et al., 2014).

The morphology and element distribution of TB05, TB10, TB20, and TB30 were observed by SEM–EDS (Fig. 3). As shown in Fig. 3a–d, there is no obvious agglomeration in the material. The crystallite sizes of TB10, TB20, and TB30 are 9.5 nm, 8.0 nm, and 6.4 nm, respectively, estimated by the Scherrer formula (Eq. 3–1). With the addition of Bi₂O₃, the grain size of the material gradually decreased (Gómez-Cerezo et al., 2014; Lakshmana Reddy et al., 2017; Malligavathy et al., 2017; Vigil-Castillo et al., 2019). It can be seen from Fig. 3g that bismuth was uniformly distributed

on the surface of the material. The content of bismuth measured by EDS spot scanning (Fig. 3b) was 8.16%, which was slightly different from that measured by the thiourea method.

$$D = \frac{K\gamma}{B cos\theta} \quad\quad (3\text{-}1)$$

where *D* is the grain diameter perpendicular to the crystal plane, nm. *K* is Scherrer's constant, generally *K* is 0.89. *λ* is the wavelength of incident X-ray, which is 0.15406 nm. *β* is the half-peak width of the diffraction peak, rad. *θ* is the Bragg diffraction angle, degree.

The band gap energies of the prepared samples are shown in Fig. 4. The band gap energies of TB05, TB10, TB20, and TB30 were 3.02, 2.98, 2.85, and 2.72 eV, respectively. With the increase of Bi₂O₃ content, the band gap of the material gradually decreased and the optical absorption range gradually increased. After adding Bi₂O₃, the light absorption of the material was enhanced obviously and the spectrum was similar (the shoulder typically of Bi₂O₃ (Tang et al., 2021)). Meanwhile, due to the strong coordination effect of p-n heterojunction, the band gap of the material was shortened from 3.02 to 2.72 eV. Compared with pure TiO₂, the composite photocatalyst was easier to excite under visible light irradiation.
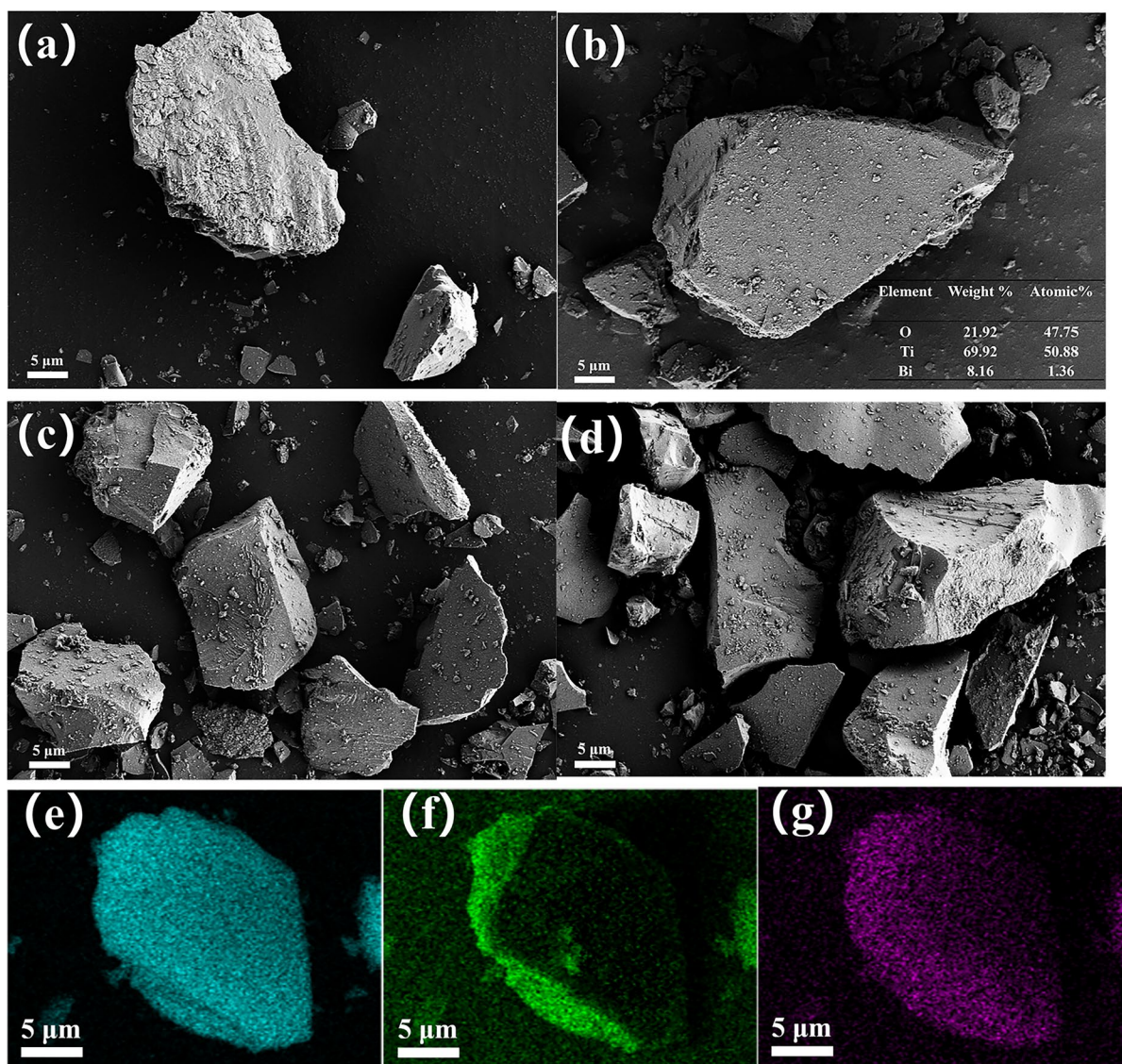
Element	Weight %	Atomic%
O	21.92	47.75
Ti	69.92	50.88
Bi	8.16	1.36

Fig. 3 SEM–EDS of samples. SEM images of TB05, TB10, TB20, and TB30 (**a–d**). EDS mapping of TB10 sample (**e** Ti, **f** O, **g** Bi), the inset shows atomic ratios for TB10

3.2 Adsorption Study

Figure 5 shows the effect of contact time on the adsorption of AR18 by TiO$_2$, TB05, TB10, TB20, and TB30. The adsorption capacity of TiO$_2$ to AR18 was extremely low, and the adsorption capacity of TB05, TB10, TB20, and TB30 to AR18 was 9 mg/g, 24 mg/g, 16 mg/g, and 11 mg/g, respectively. The addition of Bi$_2$O$_3$ further improved the adsorption capacity of TiO$_2$. Moreover, the adsorption rate was faster in the first 5 min because the adsorption process was at an early stage and there were more adsorption sites. As the contact time increased, the repulsion between the solute and bulk phase made it difficult to occupy the remaining adsorption sites (Zhang et al., 2021a, 2021b). Finally, adsorption equilibrium was reached at 20 min.
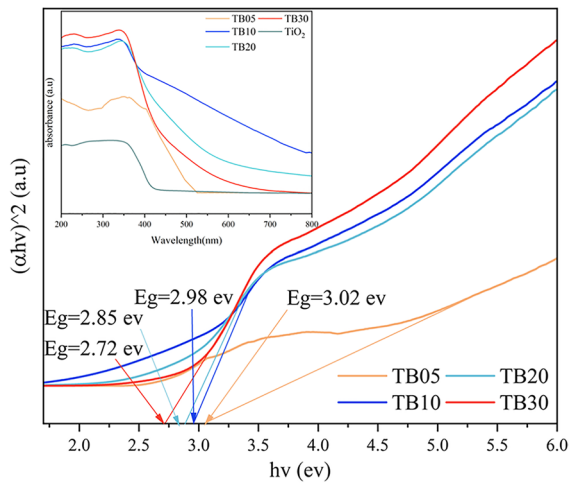
Fig. 4 The band gap energies of TB05, TB10, TB20, and TB30, the inset shows the UV–vis diffuse reflectance spectra of TiO_2, TB05, TB10, TB20, and TB30
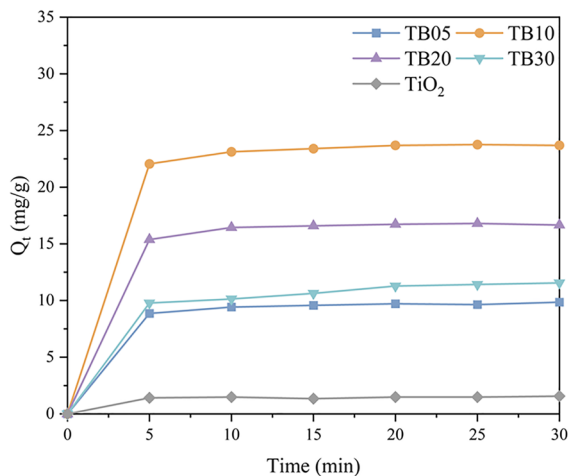

Fig. 5 Adsorption curves of AR18 by TB05, TB10, TB20, and TB30

3.3 Photocatalytic Performance Analysis

Figure 6A shows that when the dye concentration was 50 mg/L and the catalyst dosage was 50 mg, the degradation effect of different photocatalysts was on AR18. After 210 min illumination, the degradation rate of AR18 was 0 without any catalyst, indicating that the self-degradation of AR18 could be ignored. After 30-min dark adsorption, the AR18 solution concentration treated with TiO_2, Bi_2O_3, TB05, TB10,

TB20, and TB30 decreased by 1.51%, 2.39%, 15.21%, 32.07%, 21.57%, and 17.60%, respectively. This indicates that TiO_2 had poor adsorption capacity. In addition, the addition of Bi_2O_3 improved the adsorption capacity of the material (Vigil-Castillo et al., 2019). In different mass of Bi_2O_3 composite TiO_2 materials, the TB10 adsorption effect was the best, indicating that the appropriate amount of Bi_2O_3 addition could improve the adsorption properties of composite materials. Therefore, the composite of Bi_2O_3 under visible light can improve the photocatalytic performance of TiO_2. Among the materials, TB10 showed the best photocatalytic performance, and the degradation rate of AR18 could reach 99.76%. Due to the addition of Bi_2O_3, the heterojunction was formed with TiO_2, and the separation of electrons and holes were promoted by the spatial potential difference. At the same time, the narrow optical response range, poor optical absorption ability, and low quantum efficiency of TiO_2 were improved (Low et al., 2017; Tai et al., 2022), and the degradation efficiency of AR18 was improved. To further studying the photocatalytic degradation process, the photocatalytic degradation kinetics was studied. The pseudo-first-order dynamic equation is shown in Eq. 3–2.

$$\ln\left(C_0/C_t\right) = kt \tag{3-2}$$

where k is the pseudo-first-order reaction rate constant (min^{-1}), t is the light irradiation time (min), C_0 is the concentration of AR18 solution following dark adsorption (mg/L), and C_t is the concentration of AR18 solution after light irradiation for time t (mg/L).

Figure 6b shows the results obtained after fitting. The degradation of AR18 by composites with different mass ratios of Bi_2O_3 accorded with the pseudo-first-order kinetic equation. The degradation rate of AR18 by Bi_2O_3 was relatively low. The p-n heterojunction formed between Bi_2O_3 and TiO_2 improved the removal rate of AR18. When the mass of Bi_2O_3 was 10%, the k value reached the maximum and TB10 showed the highest activity. Aggregation of excessive Bi_2O_3 resulted in a slight decrease in photocatalytic activity of the material (Chang et al., 2017; Zou et al., 2019). Compared with the degradation efficiency of other reported bismuth titanium materials (Table 1), TB10 prepared by the sol–gel method showed excellent removal ability (99.76%) for AR18 (50 mg/L,
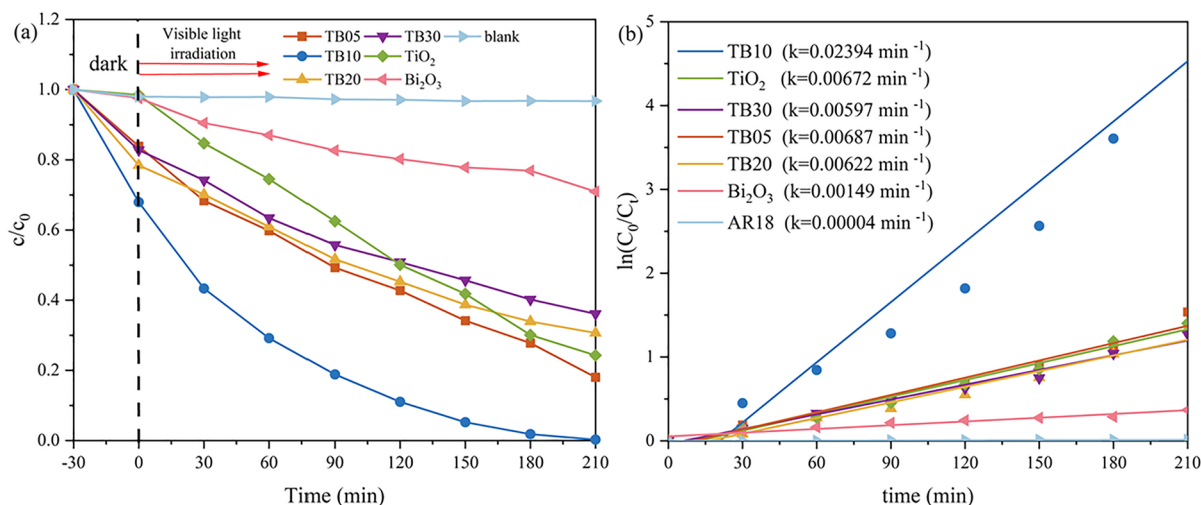
Fig. 6 AR18 photocatalytic degradation curve (**a**) fitting graph of the pseudo-first-order kinetic equation (**b**)

Table 1 Comparison of photocatalyst with other similar reported system

Sample	Catalyst dosage	Pollutant concentration	Irradiation time	Efficiency	Ref
BiOI/Bi/TiO$_2$	-	RhB -	330 min	97.3%	(Zhang et al., 2022)
TiO$_2$/Bi$_5$O$_7$I	40 mg	RhB 40 mL (10 mg/L)	120 min	90%	(Mai et al., 2022)
Bi/TiO$_2$/WO$_3$·0.33H$_2$O	10 mg	RhB 40 mL (10 mg/L)	90 min	99.84%	(Deng et al., 2020)
TiO$_2$/BiVO	5 mg	MB 20 mL (5 mg/L)	300 min	96.23%	(Soares et al., 2022)
TiO$_2$-WO$_3$-Bi$_2$O$_3$/SiO$_2$	10 mg	RhB 10 mL (10 mg/L)	240 min	92%	(Haghighi et al., 2022)
Bi$_2$S$_3$/BiVO$_4$/TiO$_2$	-	MO -	180 min	76.4%	(Liu et al., 2021)
TB 10	50 mg	AR18 100 mL (50 mg/L)	240 min	99.76%	This work

100 mL) through the synergistic effect of adsorption and photocatalysis within 240 min, indicating it is a promising environmental functional material.

3.4 Analysis of affecting factors the photocatalytic experiment

3.4.1 Catalyst Dosage

In order to discuss the influence of catalyst dosage on the photocatalytic degradation of AR18 by TB10, 10, 30, 50, 80, and 100 mg, catalysts were added to 100 mL AR18 solution (50 mg/L), respectively. The results are shown in Fig. 7. With the increase of catalyst dosage, the degradation rate of AR18 dye gradually increased. When the catalyst dosage was 0.01 g, the amount of catalyst was less, and the hole h_{vb}^+ and highly active superoxide radical ($\bullet O_2^-$) generated in
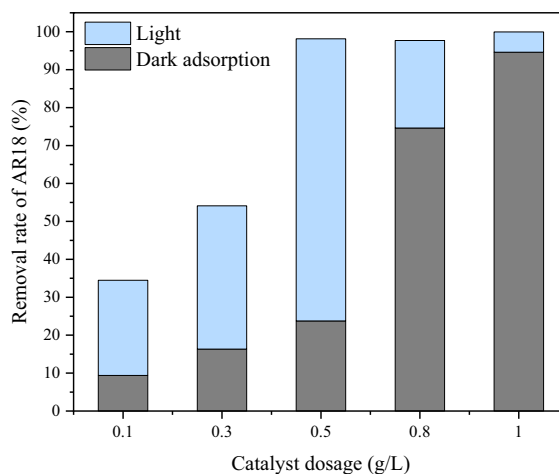

Fig. 7 Effect of catalyst dosage on AR18 degradation

unit time were less, so the degradation rate of dyes was low (An et al., 2020). Dark adsorption increases with the increase of dosage and the photodegradation increased from 21.1 to 37.8%, then reached the maximum value (74.4%) and then gradually decreased to 5.4% with the increase of dosage. When the dosage was 0.5 g/L, the photodegradation was the best, and the value was 74.38%. Therefore, the optimal dosage of catalyst is 0.5 g/L for 50 mg/L AR18 solution.

3.4.2 Initial Dye Concentration

To study the effect of initial dye concentration on the photocatalytic degradation of AR18 by TB10, 50 mg TB10 was added to 40, 50, 60, 70, and 80 mg/L AR18 solution (100 mL), respectively. The results are shown in Fig. 8. With the increase of initial dye concentration, the degradation rate of AR18 decreased gradually after the same treatment time. When the initial dye concentration was 80 mg/L, the degradation rate of AR18 was only 34.75% after 210 min illumination. While when the initial dye concentration was 50 mg/L, the degradation rate was 98.6% and the solution was colorless. At first, with the increase of dye concentration, the AR18 solution obstructed light irradiation on the catalyst, so the actual incident light intensity on the catalyst surface decreased, resulting in a corresponding decrease in the amount of $\bullet O_2^-$ (Ji et al., 2021). Secondly, when the AR18 dye concentration was too high, the AR18 molecules collided with each other in the reaction vessel (Xiang et al.,
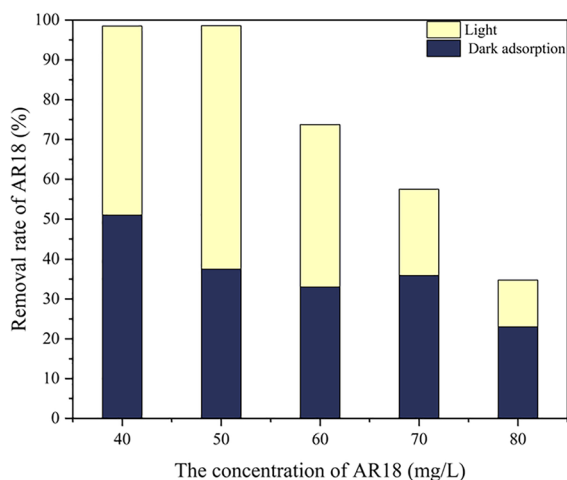
2022), a large number of photons were absorbed in the AR18. As a result, the dye molecules adsorbed in TB10 catalyst surface could not obtain enough photon energy. Finally, with the increase of dye concentration, the number of intermediate products generated by the reaction also increased and competitive adsorption occurred between intermediate products (Mahendran & Gogate, 2021) and dyes that led to the decrease of photocatalytic activity sites acting on dye molecules and the decrease of dye degradation rate. Hence, when the catalyst dosage is 0.5 g/L, the initial dye concentration should not be higher than 50 mg/L.

3.4.3 Initial Solution pH

Figure 9A displays the effect of initial pH (2–12) of dye solutions on AR18 (50 mg/L) photodegradation in the presence of TB10 (0.5 g/L). Obviously, the solution pH greatly affected the degradation efficiency of AR18. When the initial pH of dye solution decreased from 12, 9, 6.5, 5, to 2, the degradation efficiency of AR18 changed from 36.99%, 48.63%, 98.73%, 98.15%, to 90.5% in 210 min. The point of zero charge (PZC) of TB10 was estimated by the zeta potential measurement, which was at about pH 3.1 (Fig. 9b). Thereby, the surface charge of the catalyst is positive when pH < 3.1, and it becomes more negative with higher pH value when pH > 3.1. In addition, AR18 is anionic dye (Parsa et al., 2014). When the pH was reduced from 12 to 5, the electrostatic repulsion between AR18 and TB10 was weakened, thereby increasing the photodegradation rate of AR18. However, when the solution pH is 2, part of AR18 may be protonated and positively charged. As a result, photodegradation of AR18 decreased. The similar result was observed in the photocatalytic degradation of direct red 16 dye using L-cysteine-TiO$_2$/Bi$_2$O$_3$ (Karimzadeh & Bahrami, 2022).

3.4.4 The Stability and Recyclability Test

The reusability of TB10 was evaluated by cyclic synergistic adsorption-photodegradation to remove AR18, as shown in Fig. 10. The removal ratio of AR18 was almost 100% for the first time. However, the removal ratio decreased in the second time in which 90% of AR18 was removed after 240 min. In the third time of removal, only 79% of AR18 was removed after 240 min. The reduction of activity may
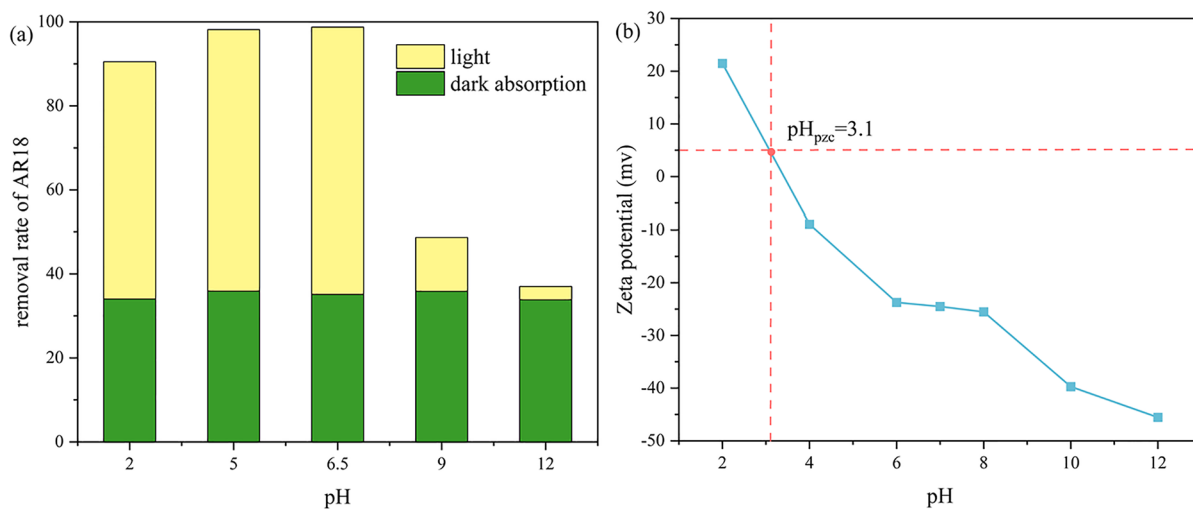

Fig. 8 Effect of initial dye concentration on AR18 degradation

Fig. 9 Effect of pH on degradation of acid red 18 (**a**). Zeta potential of TB10 (**b**)
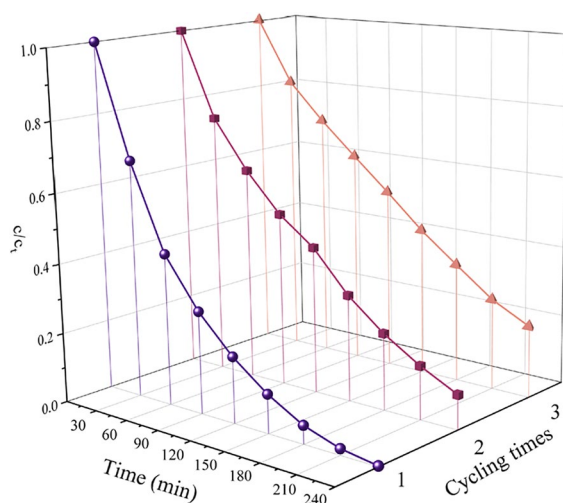

Fig. 10 The reusability of TB10

be related to the mass loss of catalyst during experiments and the blockage of active sites by the adsorption of intermediaries in degradation or AR18 molecules (Luo et al., 2022a, 2022b, 2022c, 2022d).

3.5 Analysis of Degradation Mechanism

At first, p-benzoquinone (PBQ), potassium iodide (KI), and tert-butyl alcohol (TBA) were used as the trapping agents for superoxide radical ($\bullet O_2^-$), hole (h^+), and hydroxyl radical ($\bullet OH$), respectively. The results are shown in Fig. 11a. The degradation rate of AR18 after adding TBA in the reaction system was 99.89%, indicating that $\bullet OH$ was not the main active species. After adding KI and PBQ, the degradation rate of AR18 was significantly reduced 18.02% and 78.12%, respectively, indicating that the main active species are h^+ and $\bullet O_2^-$.

To further verify the strength of the two free radicals, ESR spectra were recorded using DMPO and TEMOP as a spin trapping agent. The DMPO $\bullet O_2^-$ was not observed under dark conditions. The signal intensity of DMPO $\bullet O_2^-$ increased when illumination was applied after 30 min of illumination, and the DMPO $\bullet O_2^-$ spin adduct has a characteristic quartet of 1:1:1:1 intensity ratio (Fig. 11b) (Luo et al., 2022a, 2022b, 2022c, 2022d; Zhao et al., 2020). In addition, the weakening of the hole peak after illumination (Fig. 11c). This was due to the holes generated and reacted with TEMPO under light illumination, resulting in the weak of the peak intensity of TEMPO signal (Luo et al., 2022a, 2022b, 2022c, 2022d). Therefore, ESR spectra further confirmed that $\bullet O_2^-$ and h^+ are the dominant active oxidative species.

Based on these, the photodegradation mechanism of AR18 degradation on TB10 was proposed. As shown in Fig. 12, when p-type Bi_2O_3 contacted with TiO_2, due to the potential difference, electrons would transfer from n-type TiO_2 to p-type Bi_2O_3, while holes would transfer from Bi_2O_3 to TiO_2 until the Fermi level balance of the system was completed (Low et al., 2017; Rajendran et al., 2022; Tang et al.,
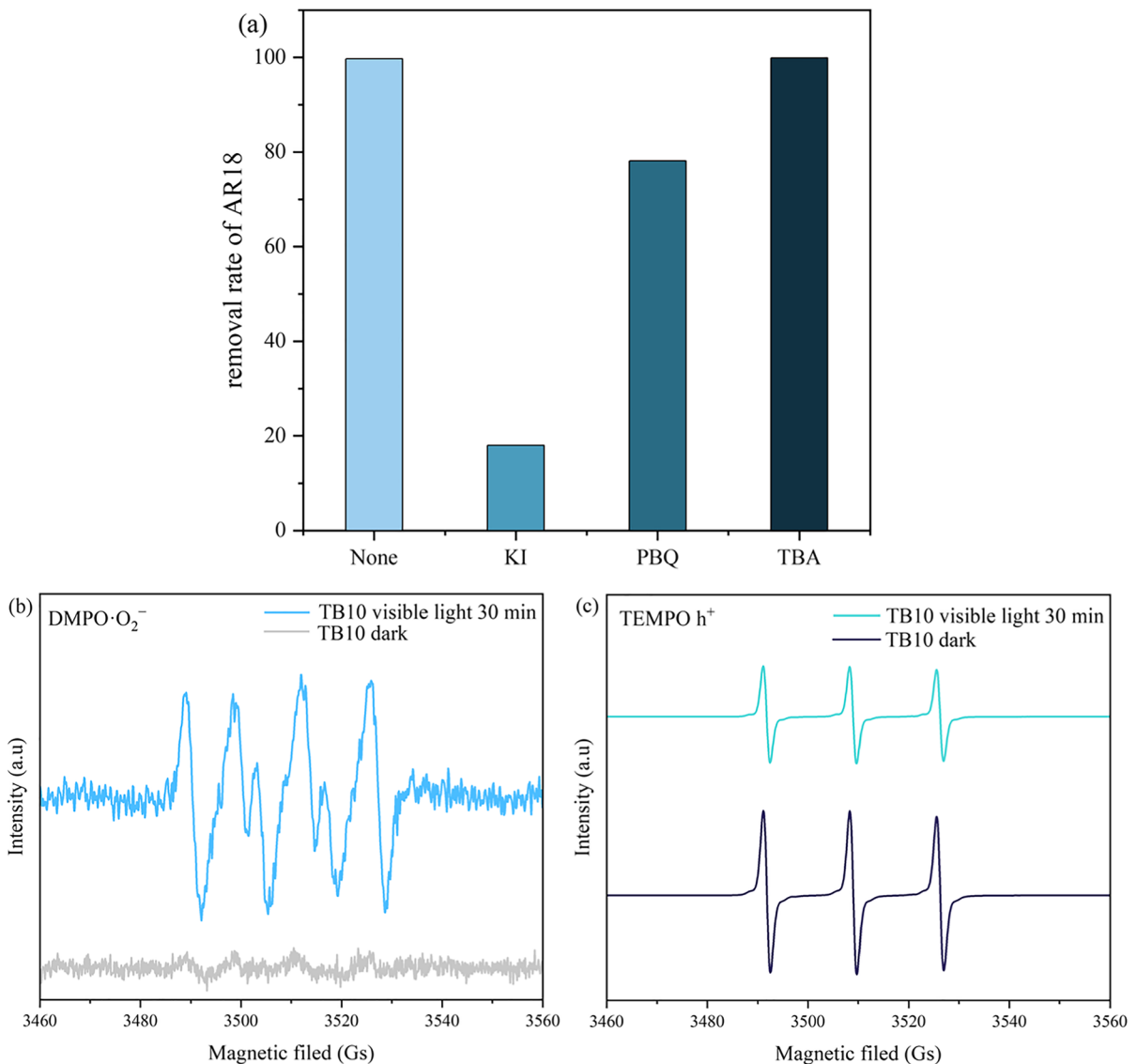
Fig. 11 Scavenger experiments of TB10 (**a**). ESR spectra of DMPO·O$_2^-$ and TEMPO h.$^+$ in TB10 (**b**, **c**)

2021). Due to its small energy gap, Bi$_2$O$_3$ was easily excited and generated electrons and holes under visible light. Subsequently, the electrons on the Bi$_2$O$_3$ conduction band (CB) rapidly migrated to the TiO$_2$ conduction band and then participated in the generation of active species. In addition, the holes left on the valence band (VB) of Bi$_2$O$_3$ directly oxidized AR18. As a result of the formation of p-n heterojunction, photogenerated electrons could transfer rapidly, thus prolonging the carrier lifetime and decreasing the recombination of e$^-$/h$^+$ pairs (Wen et al., 2019).

4 Conclusions

(1) XRD, SEM–EDS, and other characterization methods proved that Bi$_2$O$_3$ and TiO$_2$ were successfully compounded by the sol–gel method, and the effect of Bi$_2$O$_3$ content on the photocatalytic performance of the material was studied. UV–Vis DRS analysis showed that TB10 had a great enhancement in the absorption of visible light and ultraviolet light compared with TiO$_2$, and the absorption band had a bathochromic shift.
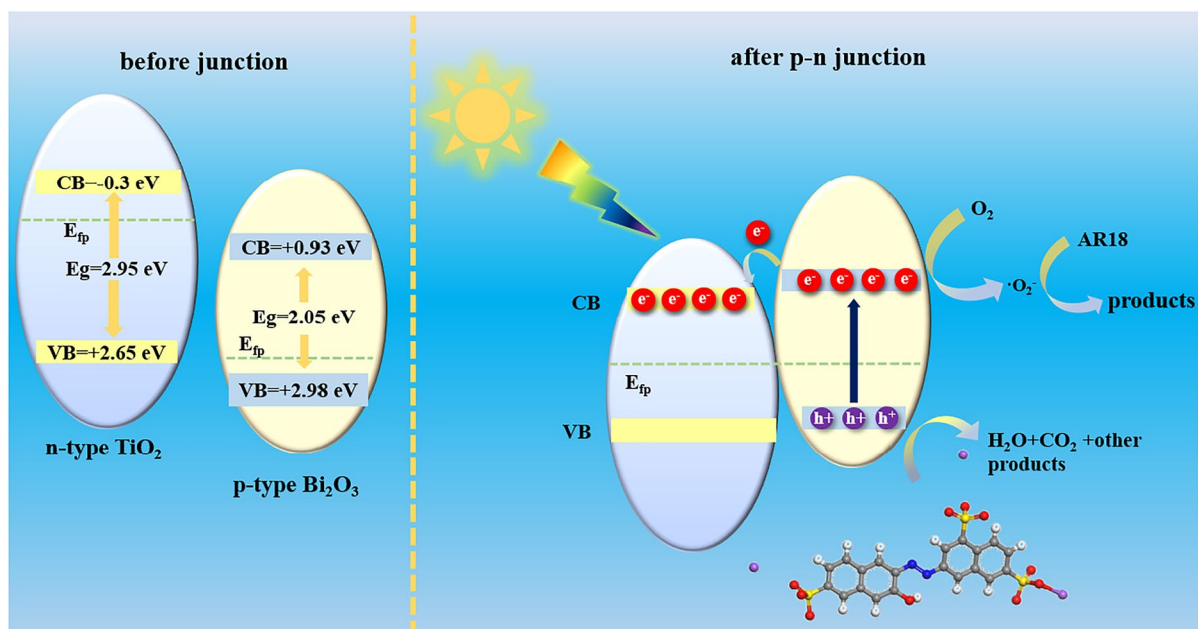
Fig. 12 Mechanism of photocatalytic degradation of acid red 18 by TB10

The band gap was 2.98 eV, manifesting that TB10 had high photocatalytic activity. (2) The photocatalytic degradation of AR18 by p-n type heterojunctions Bi_2O_3/TiO_2 accords with pseudo first order kinetic equation. The optimal degradation condition was that the initial concentration of the solution was 50 mg/L, the catalyst dosage was 0.5 g/L, and the pH was 6.5. Under this condition, the decolorization rate of AR18 was 99.76%. What calls for special attention is that TB10 can show good catalytic performance under unadjusted pH conditions. The main active species in this photocatalytic process are h^+ and $\bullet O_2^-$. (3) The main reason for the improvement of photocatalytic activity is that the composite of Bi_2O_3 and TiO_2 expands the light response range of the composite (including the visible light wavelength). The p-n heterojunction formed between Bi_2O_3 and TiO_2 effectively promotes the separation of e^-/h^+. The addition of Bi_2O_3 increased the specific surface area of the composites and played a positive role in photocatalysis. This study provides a new way to improve the ability of TiO_2 to treat dye wastewater.

Data availability The datasets used or analyzed during study are available from corresponding author on reasonable request

Declarations

Conflict of interest The other authors declare that they have no known competing financial interests or personal relationships that could have appeared to influence the work reported in this paper.

References

An, W., Tian, L., Hu, J., Liu, L., Cui, W., & Liang, Y. (2020). Efficient degradation of organic pollutants by catalytic ozonation and photocatalysis synergy system using double-functional MgO/g-C3N4 catalyst. *Applied Surface Science, 534*, 147518. https://doi.org/10.1016/j.apsusc.2020.147518

Arutanti, O., Sari, A. L., Kartikowati, C. W., Sari, A. A., & Arif, A. F. (2022). Design and application of homogeneous-structured TiO_2/activated carbon nanocomposite for adsorption–photocatalytic degradation of MO. *Water, Air, & Soil Pollution, 233*, 118. https://doi.org/10.1007/s11270-022-05600-1

Cervantes-Aviles, P., Camarillo, P. N., Ida, J., & Cuevas-Rodriguez, G. (2017). Influence of wastewater type on the impact generated by TiO_2 nanoparticles on the oxygen uptake rate in activated sludge process. *Journal of Environmental Management, 190*, 35–44. https://doi.org/10.1016/j.jenvman.2016.12.054

Chang M, Hu H, Zhang Y, Chen D, Wu L, Li X. (2017). Improving visible light-absorptivity and photoelectric conversion efficiency of a TiO_2 nanotube anode film by sensitization with Bi_2O_3 nanoparticles. *Nanomaterials (Basel), 7*, 104. https://doi.org/10.3390/nano7050104

Cheng, L., & Kang, Y. (2014). Selective preparation of Bi_2O_3 visible light-driven photocatalyst by dispersant and calcination. *Journal of Alloys and Compounds, 585*, 85–93. https://doi.org/10.1016/j.jallcom.2013.08.010

Deng, Y., Zhou, Y., Tang, H., Xu, Y., Tan, Y., Zou, H., & Xiang, Y. (2020). Synthesis of Z-scheme Bi/TiO_2/$WO_3 \cdot 0.33H2O$ heterojunction material for the enhanced photocatalytic degradation of pollutants. *Journal of Materials Science: Materials in Electronics, 31*, 11276–11285. https://doi.org/10.1007/s10854-020-03676-1

Ge, M., Hu, Z., Wei, J., He, Q., & He, Z. (2021). Recent advances in persulfate-assisted TiO_2-based photocatalysis for wastewater treatment: Performances, mechanism and perspectives. *Journal of Alloys and Compounds, 888*, 161625. https://doi.org/10.1016/j.jallcom.2021.161625

Gómez-Cerezo, M. N., Muñoz-Batista, M. J., Tudela, D., Fernández-García, M., & Kubacka, A. (2014). Composite Bi_2O_3–TiO_2 catalysts for toluene photo-degradation: Ultraviolet and visible light performances. *Applied Catalysis b: Environmental, 156–157*, 307–313. https://doi.org/10.1016/j.apcatb.2014.03.024

Haghighi, P., Alijani, S., Bazyari, A., & Thompson, L. T. (2022). Visible light dye degradation over fluorinated mesoporous $TiO_2 − WO_3 − Bi_2O_3$/SiO_2 nanocomposite photocatalyst-adsorbent using immersion well reactor. *Journal of Photochemistry and Photobiology a: Chemistry, 426*, 113790. https://doi.org/10.1016/j.jphotochem.2022.113790

Ji, S., Yang, Y., Zhou, Z., Li, X., & Liu, Y. (2021). Photocatalysis-fenton of Fe-doped g-C3N4 catalyst and its excellent degradation performance towards RhB. *Journal of Water Process Engineering, 40*, 101804. https://doi.org/10.1016/j.jwpe.2020.101804

Karimzadeh, S., & Bahrami, K. (2022). Investigation of the photocatalytic activity of a novel-driven photocatalyst L-cysteine-TiO_2/Bi_2O_3 under visible light irradiation: Process optimization and modeling. *INT J ENVIRON SCI TE, 19*, 3715–3730. https://doi.org/10.1007/s13762-021-03516-7

Khalid, N. R., Majid, A., Tahir, M. B., Niaz, N. A., & Khalid, S. (2017). Carbonaceous-TiO_2 nanomaterials for photocatalytic degradation of pollutants: A review. *Ceramics International, 43*, 14552–14571. https://doi.org/10.1016/j.ceramint.2017.08.143

Lakshmana Reddy, N., Emin, S., Valant, M., & Shankar, M. V. (2017). Nanostructured Bi_2O_3@TiO_2 photocatalyst for enhanced hydrogen production. *INT J HYDROGEN ENERG, 42*, 6627–6636. https://doi.org/10.1016/j.ijhydene.2016.12.154

Liu, Z., Xu, K., Yu, H., Zhang, M., & Sun, Z. (2021). In-situ preparation of double Z-scheme $Bi2S3/BiVO_4/TiO_2$ ternary photocatalysts for enhanced photoelectrochemical and photocatalytic performance. *Applied Surface Science, 545*, 148986. https://doi.org/10.1016/j.apsusc.2021.148986

Lou, B., Chen, C., Liu, J., Zou, S., Xiao, L., & Fan, J. (2021). Selectively depositing Bi_2O_3 quantum dots on TiO_2 nanotubes for efficient visible-light-driven photocatalysis. *Materials Letters, 288*, 129413. https://doi.org/10.1016/j.matlet.2021.129413

Low, J., Yu, J., Jaroniec, M., Wageh, S., & Al-Ghamdi, A. A. (2017). *Heterojunction Photocatalysts. ADV MATER, 29*, 1601694. https://doi.org/10.1002/adma.201601694

Luo, Y., Han, Y., Hua, Y., Xue, M., Yu, S., Zhang, L., Yin, Z., Li, X., Ma, X., Wu, H., Liu, T., Shen, Y., & Gao, B. (2022a). Step scheme nickel-aluminium layered double hydroxides/biochar heterostructure photocatalyst for synergistic adsorption and photodegradation of tetracycline. *Chemosphere, 309*, 136802. https://doi.org/10.1016/j.chemosphere.2022.136802

Luo, Y., Han, Y., Xue, M., Xie, Y., Yin, Z., Xie, C., Li, X., Zheng, Y., Huang, J., Zhang, Y., Yang, Y., & Gao, B. (2022b). Ball-milled bismuth oxybromide/biochar composites with enhanced removal of reactive red owing to the synergy between adsorption and photodegradation. *Journal of Environmental Management, 308*, 114652. https://doi.org/10.1016/j.jenvman.2022.114652

Luo, Y., Zheng, A., Xue, M., Xie, Y., Yu, S., Yin, Z., Xie, C., Hong, Z., Tan, W., Zou, W., Dong, L., & Gao, B. (2022c). Ball-milled Bi_2MoO_6/biochar composites for synergistic adsorption and photodegradation of methylene blue: Kinetics and mechanisms. *Industrial Crops and Products, 186*, 115229. https://doi.org/10.1016/j.indcrop.2022.115229

Luo YD, Wang YH, Zhu YW, Xue MS, Zheng AF, Han Y, Yin ZZ, Hong Z, Xie C, Li XB, Lei S, Gao B. (2022d). Ball-milled bismuth oxychloride/biochar nanocomposites with rich oxygen vacancies for reactive red-120 adsorption in aqueous solution. *BIOCHAR, 4*, 21. https://doi.org/10.1007/s42773-022-00147-0

Mahendran, V., & Gogate, P. R. (2021). Degradation of acid scarlet 3R dye using oxidation strategies involving photocatalysis based on Fe doped TiO_2 photocatalyst, ultrasound and hydrogen peroxide. *Separation and Purification Technology, 274*, 119011. https://doi.org/10.1016/j.seppur.2021.119011

Mai, X., Lin, W., Chen, J., Yang, Q., & Gao, R. (2022). Synthesis of Z-scheme (001)-TiO_2/Bi_5O_7I heterojunctions

with enhanced interfacial charge separation and photocatalytic degradation of Rhodamine B. *Reaction Kinetics, Mechanisms and Catalysis, 135*, 3447–3459. https://doi.org/10.1007/s11144-022-02309-4

Malligavathy, M., Iyyapushpam, S., Nishanthi, S. T., & Pathinettam, P. D. (2017). Remarkable catalytic activity of Bi_2O_3/TiO_2 nanocomposites prepared by hydrothermal method for the degradation of methyl orange. *Journal of Nanoparticle Research, 19*, 144. https://doi.org/10.1007/s11051-017-3806-x

Meda, U. S., Vora, K., Athreya, Y., & Mandi, U. A. (2022). Titanium dioxide based heterogeneous and heterojunction photocatalysts for pollution control applications in the construction industry. *PROCESS SAF ENVIRON, 161*, 771–787. https://doi.org/10.1016/j.psep.2022.03.066

Mejía-Morales, C., Hernández-Aldana, F., Cortés-Hernández, D. M., Rivera-Tapia, J. A., Castañeda-Antonio, D., & Bonilla, N. (2020). Assessment of biological and persistent organic compounds in hospital wastewater after advanced oxidation process $UV/H_2O_2/O_3$. *Water, Air, & Soil Pollution, 231*, 89. https://doi.org/10.1007/s11270-020-4463-8

Mishra, A., Kumari, M., Swati, K. R., Iqbal, K., & Thakur, I. S. (2022). Persistent organic pollutants in the environment: Risk assessment, hazards, and mitigation strategies. *Bioresource Technology Reports, 19*, 101143. https://doi.org/10.1016/j.biteb.2022.101143

Parsa, J. B., Golmirzaei, M., & Abbasi, M. (2014). Degradation of azo dye C.I. Acid Red 18 in aqueous solution by ozone-electrolysis process. *Journal of Industrial and Engineering Chemistry, 20*, 689–694. https://doi.org/10.1016/j.jiec.2013.05.034

Răileanu M, Crişan M, Niţoi I, Ianculescu A, Oancea P, Crişan D, Todan L. (2013). TiO_2-based nanomaterials with photocatalytic properties for the advanced degradation of xenobiotic compounds from water. A literature survey. *Water, Air, & Soil Pollution, 224,* 1548. https://doi.org/10.1007/s11270-013-1548-7

Rajendran, S., Hoang, T., Trudeau, M. L., Jalil, A. A., Naushad, M., & Awual, M. R. (2022). Generation of novel n-p-n (CeO_2-PPy-ZnO) heterojunction for photocatalytic degradation of micro-organic pollutants. *Environmental Pollution, 292*, 118375. https://doi.org/10.1016/j.envpol.2021.118375

Ren, C., Qiu, W., Zhang, H., He, Z., & Chen, Y. (2015). Degradation of benzene on $TiO_2/SiO_2/Bi_2O_3$ photocatalysts under UV and visible light. *Journal of Molecular Catalysis a: Chemical, 398*, 215–222. https://doi.org/10.1016/j.molcata.2014.12.007

Rongan, H., Haijuan, L., Huimin, L., Difa, X., & Liuyang, Z. (2020). S-scheme photocatalyst Bi_2O_3/TiO_2 nanofiber with improved photocatalytic performance. *Journal of Materials Science and Technology, 52*, 145–151. https://doi.org/10.1016/j.jmst.2020.03.027

Soares FC, Almeida J, Koga RH, Duque D, Silva G, Ribeiro C, Mendonca V. (2022). $TiO_2/BiVO_4$ composite from preformed nanoparticles for heterogeneous photocatalysis. *Mater Chem Phys, 290*, 126588. https://doi.org/10.1016/j.matchemphys.2022.126588

Taddesse, A. M., Alemu, M., & Kebede, T. (2020). Enhanced photocatalytic activity of p-n-n heterojunctions ternary composite $Cu_2O/ZnO/Ag_3PO_4$ under visible light irradiation. *Journal of Environmental Chemical Engineering, 8*, 104356. https://doi.org/10.1016/j.jece.2020.104356

Tai, X. H., Lai, C. W., Yang, T. C. K., Johan, M. R., Lee, K. M., Chen, C., & Juan, J. C. (2022). Highly effective removal of volatile organic pollutants with p-n heterojunction photoreduced graphene oxide-TiO_2 photocatalyst. *Journal of Environmental Chemical Engineering, 10*, 107304. https://doi.org/10.1016/j.jece.2022.107304

Tang, T., Yin, Z., Chen, J. R., Zhang, S., Sheng, W., Wenxian Wei, C., Xiao, Y., Shi, Q., & Cao, S. (2021). Novel p-n heterojunction Bi_2O_3_Ti_3+-TiO_2 photocatalyst enables the complete removal of tetracyclines under visible light. *Chemical Engineering Journal, 417*, 128058. https://doi.org/10.1016/j.cej.2020.128058

Valencia, G. K., López, A., Hernández-Gordillo, A., Zanella, R., & Rodil, S. E. (2018). Stabilized β-Bi_2O_3 nanoparticles from $(BiO)_4CO_3(OH)_2$ precursor and their photocatalytic properties under blue light. *Ceramics International, 44*, 22329–22338. https://doi.org/10.1016/j.ceramint.2018.08.358

Vigil-Castillo, H. H., Hernández-Ramírez, A., Guzmán-Mar, J. L., Ramos-Delgado, N. A., & Villanueva-Rodríguez, M. (2019). Performance of Bi_2O_3/TiO_2 prepared by sol-gel on p-Cresol degradation under solar and visible light. *ENVIRON SCI POLLUT R, 26*, 4215–4223. https://doi.org/10.1007/s11356-018-2212-y

Wen, X., Shen, C., Fei, Z., Niu, C., Lu, Q., Guo, J., & Lu, H. (2019). Fabrication of a zinc tungstate-based a p-n heterojunction photocatalysts towards refractory pollutants degradation under visible light irradiation. *Colloids and surfaces. A, Physicochemical and Engineering Aspects, 573*, 137–145. https://doi.org/10.1016/j.colsurfa.2019.04.026

Wu, Y., Meng, D., Guo, Q., Gao, D., & Wang, L. (2022). Study on TiO_2/g-C3N4 S-Scheme heterojunction photocatalyst for enhanced formaldehyde decomposition. *Optical Materials, 126*, 112213. https://doi.org/10.1016/j.optmat.2022.112213

Xiang, H., Tuo, B., Tian, J., Hu, K., Wang, J., Cheng, J., & Tang, Y. (2021). Preparation and photocatalytic properties of Bi-doped TiO_2/montmorillonite composite. *Optical Materials, 117*, 111137. https://doi.org/10.1016/j.optmat.2021.111137

Xiang, D., Lu, S., Ma, Y., & Zhao, L. (2022). Synergistic photocatalysis-fenton reaction of flower-shaped CeO_2/Fe_3O_4 magnetic catalyst for decolorization of high concentration congo red dye. *Colloids and Surfaces a: Physicochemical and Engineering Aspects, 647*, 129021. https://doi.org/10.1016/j.colsurfa.2022.129021

Yi, W., Yan, C., Hamdy, M. S., Baltrusaitis, J., & Mul, G. (2014). Effects of bismuth addition and photo-deposition of platinum on (surface) composition, morphology and visible light photocatalytic activity of sol–gel derived TiO_2. *Applied Catalysis b: Environmental, 154–155*, 153–160. https://doi.org/10.1016/j.apcatb.2014.01.055

You, Y., Yuan, H., Wu, Y., Ma, Y., Meng, C., & Zhao, X. (2021). A novel red phosphorus/perylene diimide metal-free photocatalyst with p-n heterojunctions for efficient photoreduction of bromate under visible light. *Separation and Purification Technology, 264*, 118456. https://doi.org/10.1016/j.seppur.2021.118456

Zhang, T., Wang, W., Zhao, Y., Bai, H., Wen, T., Kang, S., Song, G., Song, S., & Komarneni, S. (2021a). Removal of heavy metals and dyes by clay-based adsorbents: From natural clays to 1D and 2D nano-composites. *Chemical Engineering Journal, 420*, 127574. https://doi.org/10.1016/j.cej.2020.127574

Zhang, Y., Yu, H., Li, S., Wang, L., Huang, F., Guan, R., Li, J., Jiao, Y., & Sun, J. (2021b). Rapidly degradation of di-(2-ethylhexyl) phthalate by Z-scheme $Bi_2O_3/TiO_2@$ reduced graphene oxide driven by simulated solar radiation. *Chemosphere, 272*, 129631. https://doi.org/10.1016/j.chemosphere.2021.129631

Zhang, C. C., Chen, W. B., Hu, D. R., Xie, H. J., Song, Y. B., Luo, B. B., Fang, Y. W., Gao, W. H., & Zhong, Z. Y. (2022). Design and in-situ construct BiOI/Bi/TiO$_2$ photocatalysts with metal-mediated heterostructures employing oxygen vacancies in TiO2 nanosheets. *GREEN ENERGY & ENVIRONMENT, 7*, 680–690. https://doi.org/10.1016/j.gee.2020.11.013

Zhao, Y., Kang, S., Qin, L., Wang, W., Zhang, T., Song, S., & Komarneni, S. (2020). Self-assembled gels of Fe-chitosan/montmorillonite nanosheets: Dye degradation by the synergistic effect of adsorption and photo-Fenton reaction. *Chemical Engineering Journal, 379*, 122322. https://doi.org/10.1016/j.cej.2019.122322

Zou, Q., Li, H., Yang, Y., Miao, Y., & Huo, Y. (2019). Bi_2O_3/TiO_2 photocatalytic film coated on floated glass balls for efficient removal of organic pollutant. *Applied Surface Science, 467–468*, 354–360. https://doi.org/10.1016/j.apsusc.2018.10.182